Eur. Phys. J. B **49**, 195–203 (2006)
DOI: 10.1140/epjb/e2006-00045-9

THE EUROPEAN PHYSICAL JOURNAL B

Short-time dynamics and critical behavior of three-dimensional bond-diluted Potts model

J.Q. Yin[1,2], B. Zheng[1,2,a], V.V. Prudnikov[3], and S. Trimper[2]

[1] Zhejiang University, Zhejiang Institute of Modern Physics, Hangzhou 310027, P.R. China
[2] FB Physik, Universität – Halle, 06099 Halle, Germany
[3] Department of Theoretical Physics, Omsk State University, Mira prospekt 55-A, Omsk 644077, Russia

Received 31 August 2005
Published online 17 February 2006 –

Abstract. The short-time dynamics of the three-dimensional bond-diluted 4-state Potts model is investigated with Monte Carlo simulations. A recently suggested nonequilibrium reweighting method is applied, and the tricritical point is determined with the short-time dynamic approach. Based on the dynamic scaling form, both the dynamic and static critical exponents are estimated for the second order phase transition. Dynamic corrections to scaling are carefully considered.

PACS. 64.60.Ht Dynamic critical phenomena – 75.40.Mg Numerical simulation studies – 64.60.Fr Equilibrium properties near critical points, Critical exponents – 05.50.+q Lattice theory and statistics (Ising, Potts, etc.)

1 Introduction

The influence of quenched disorder on phase transitions has attracted considerable interest in the field of statistical physics. Earlier theoretical works [1–3] on disordered systems indicate that quenched disorder could produce rounding of a first-order phase transition, and thus induce a second-order one. The pure Potts model exhibits a temperature-driven first- or second-order phase transition, depending on the number of states q and spatial dimension D. The disordered Potts model is therefore a good laboratory for the study of the effect of quenched disorder on phase transitions. Along this understanding, many activities in the last decade have been devoted to the disordered Potts model in two dimensions [4–12].

For the disordered Potts model in higher dimensions, theoretically it is shown that a tricritical point may appear at a finite concentration of impurities [6], and it separates the first- and second-order transitions. In three dimensions, for understanding the influence of disorder on first-order transitions, the first numerical study of the Potts models with quenched disorder was presented in reference [13], and recently, the site-diluted three-state and bond-diluted four-state Potts models [14–16] have been studied with Monte Carlo simulations. Numerical evidence for the existence of a tricritical point was reported. The tricritical point was located to be around the bond concentration $p = 0.76(8)$, and the critical exponents of the induced continuous transition are estimated [15,16]. The exponents seems to be dilution-dependent, and such a behavior is attributed to the strong corrections to scaling.

In 1989, with renormalization group methods Janssen, Schaub, and Schmittmann derived a dynamic scaling form, which is valid up to the *macroscopic short-time regime*, after a microscopic time scale t_{mic} [17]. The system initially at a high temperature state with a small magnetization is suddenly quenched to the critical temperature, and then released to the dynamic evolution of model A. Such a short-time dynamic scaling behavior has been numerically verified [18–22], and it is also consistent with relevant theories and experiments in spin glasses. Furthermore, the short-time dynamic scaling can be extended to the dynamic relaxation starting from an ordered state [21,23,24].

More interestingly, based on the short-time dynamic scaling, it is possible to extract not only the dynamic exponents, but also the static exponents as well as the critical temperature [21,25–27]. Since the measurements are carried out in the short-time regime of the dynamic evolution, the method does *not* suffer from critical slowing down. What we pay for this approach is that the measurements of the dynamic exponents and static exponents can not be separated. Therefore, the statistical errors of the static exponents include those from the dynamic exponents. However, if we are also interested in the dynamic behavior, the short-time dynamic approach is rather useful. Compared with the non-local cluster algorithms, the dynamic approach does study the dynamics local in time, and in general applies also to disordered and frustrated systems [12,25,28–30].

[a] e-mail: bozheng@zju.edu.cn

On the other hand, in the last two decades, much effort [31–35] has been devoted to the subject of reweighting techniques in Monte Carlo simulations in equilibrium. These reweighting methods have greatly improved the efficiencies of Monte Carlo simulations in many aspects. Therefore, it is rather appealing to develop a dynamic reweighting method [36]. Recently, a rather generic reweighting method for nonequilibrium Markov processes was presented by Lee and Okabe [37]. With nonequilibrium Monte Carlo simulations at a single temperature, one obtains the dynamic evolution of physical quantities at different temperatures. But it is somewhat unsatisfactory that for the procedure suggested in reference [37], the reweighting temperatures need to be fixed before simulations, and one pays extra computer times in proportion to the number of the reweighting temperatures.

The purpose of this article is to study numerically the effect of quenched randomness on the softening of the first-order phase transition, *with the short-time dynamic approach*. Using an improved dynamic reweighting technique, we perform extensive dynamic Monte Carlo simulations for the three-dimensional bond-diluted 4-state Potts model, and provide a relatively accurate estimate of the tricritical point. The short-time dynamic approach to the weak first-order phase transition and application of the dynamic reweighting methods are attractive in this context. Based on the short-time dynamic scaling form with corrections to scaling, *both static and dynamic* critical exponents of the induced continuous phase transition are extracted.

The models, the dynamic scaling analysis and an improved nonequilibrium reweighting method are described in Section 2. Numerical simulations are presented in Section 3. The final section contains the conclusions.

2 Model and method

2.1 The bond-diluted Potts model

The Hamiltonian of the three-dimensional q-state Potts model with quenched random interactions can be written as

$$-\frac{1}{k_B T}H = \sum_{<i,j>} K_{ij}\delta_{\sigma_i,\sigma_j}\ , \qquad K_{ij} > 0, \tag{1}$$

where the spin σ_i takes the values $1,\cdots\ q$, $\delta_{\sigma_i,\sigma_j}$ is the Kronecker delta function, and the sum is over nearest-neighbor pairs on a cubic lattice. For the bond-diluted case, the dimensionless couplings K_{ij} are selected from two different values of K and 0, according to a bimodal distribution,

$$P(K_{ij}) = p\delta(K_{ij} - K) + (1-p)\delta(K_{ij}). \tag{2}$$

The case of $p = 1$ corresponds to the pure Potts model.

In this paper, we study the case of $q = 4$ with the short-time dynamic approach and dynamic reweighting techniques. Monte Carlo simulations with a standard Metropolis algorithm are performed on a three-dimensional cubic lattice with periodic boundary conditions. For a review of the short-time critical dynamics and its applications, see references [21,27].

The physical observables we measure are the time-dependent magnetization, its second moment, and the auto-correlation function respectively defined as

$$M(t) = \frac{q}{(q-1)L^3}\left\langle \sum_i \left(\delta_{\sigma_i(t),1} - \frac{1}{q}\right)\right\rangle, \tag{3}$$

$$M^{(2)}(t) = \frac{q^2}{(q-1)^2L^6}\left\langle \left[\sum_i \left(\delta_{\sigma_i(t),1} - \frac{1}{q}\right)\right]^2\right\rangle, \tag{4}$$

$$A(t) = \frac{q}{(q-1)L^3}\left\langle \sum_i \left(\delta_{\sigma_i(0),\sigma_i(t)} - \frac{1}{q}\right)\right\rangle, \tag{5}$$

where L is the lattice size, and the average $\langle ... \rangle$ is over the microscopic configurations of the macroscopic initial states and the realizations of the bond-diluted couplings K_{ij}.

The static critical behavior of the three-dimensional bond-diluted 4-state Potts model has been investigated by Chatelain et al. [15,16]. Evidences are given for the existence of a tricritical point, and critical exponents in the second order transition regime are estimated with finite size scaling techniques. Our aim is to study the short-time dynamics of the model. From the short-time dynamic behavior, the transition temperatures and critical exponents will be extracted. Especially, the short-time dynamic approach to the weak first-order phase transition allows a relatively accurate estimate of the tricritical point. On the other hand, it is also interesting to improve and apply the dynamic reweighting method.

2.2 Nonequilibrium reweighting method

Ferrenberg and Swendsen [31] first introduced the histogram reweighting method in Monte Carlo simulations to calculate statistical properties of a system in equilibrium. The thermal averages for a range of temperatures can be obtained from simulations at a single temperature. Then the multi-histogram algorithm was proposed [32] to increase the effective reweighting range and minimize the statistical errors. A great improvement was achieved when the artificial ensembles were applied to the reweighting methods [33,35]. Instead of the canonical distribution of the energy histogram, a "flat" histogram was obtained. Recently, Wang and Landau [34] presented a simple method to obtain the flat histogram. These reweighting techniques have greatly improved the efficiencies of Monte Carlo simulations in equilibrium.

Very recently, a reweighting method applicable to nonequilibrium Markov processes was reported [37]. Consider a simulation up to the t-th Monte Carlo step as a sequence of states,

$$\boldsymbol{x}_t = (\sigma_1, \sigma_2, \cdots, \sigma_t), \tag{6}$$

where σ_t is the spin configuration of the system at time t. Hereafter, we refer to the Monte Carlo step simply as the time of simulation. At an inverse temperature $\beta = 1/k_{\rm B}T$, the dynamical thermal average of an observable $O(t)$ can be obtained by $\langle O(t)\rangle_\beta = (1/n)\sum_{j=1}^{n} O(\sigma_t^j)$, where σ_t^j are the spin configurations from $\{\boldsymbol{x}_t^j, j = 1, \cdots, n\}$, a set of paths obtained in the simulations at a fixed β. To calculate the dynamical thermal average at another inverse temperature β', the measured observable $O(\sigma_t^j)$ has to be reweighted with a set of weights $\{w_t^j\}$. For the same set of paths $\{\boldsymbol{x}_t^j\}$, the thermal average at β' is obtained as

$$\langle O(t)\rangle_{\beta'} = \sum_{j=1}^{n} w_t^j O(\sigma_t^j) / \sum_{j=1}^{n} w_t^j. \tag{7}$$

Here the weights w_t^j can be obtained by

$$w_{t+1}^j = \frac{P_{\beta'}(\sigma_{t+1}^j|\sigma_t^j)}{P_\beta(\sigma_{t+1}^j|\sigma_t^j)} w_t^j \text{ with } w_1^j = 1 \tag{8}$$

where the $P(\sigma_{t+1}^j|\sigma_t^j)$ is the transition probability of the Monte Carlo algorithm.

However, if the weights are directly updated in the algorithm as in reference [37], one need predetermine the reweighting temperatures. The more temperatures we intend to reweight, the more computer time it will take in the simulation. Especially, in some cases one is not sure which temperatures are needed before the simulations. To improve the algorithm, we propose the following algorithm to calculate the weights.

1. Choose a spin and flip it according to the Metropolis algorithm, with a transition probability $P_\beta(\sigma'^j|\sigma_t^j) = \min[1, \exp(-\beta\Delta E)]$. Here, ΔE is the energy change due to the trial spin flip from σ_t^j to σ'^j.
2. At this point, there are three possible outcomes,
   (a) if $\Delta E \leq 0$, the trial spin flip is always accepted and we need do nothing;
   (b) if $\Delta E > 0$ and the trial spin flip is accepted, we add 1 to $n_b^j(\Delta E, t)$;
   (c) if $\Delta E > 0$ and the trial spin flip is rejected, we add 1 to $n_c^j(\Delta E, t)$.

   Here, $n^j(\Delta E, t)$ is a function to count the number of a certain energy change ΔE up to time t in the path j. $n^j(\Delta E, t)$ should be updated in every spin flip, but recorded only at the time steps when the measurements are performed.

Obviously, the set of weights w_t^j depend on the simulation temperature β, the new temperature β' and the energy change ΔE, but not on the concrete spin configuration. We can restore different sets of weights at different temperatures from the same set of ΔE by

$$w_t^j = \prod_{\Delta E} \exp(-(\beta' - \beta) n_b^j(\Delta E, t)\Delta E) \times \prod_{\Delta E} \left[\frac{1 - \exp(-\beta'\Delta E)}{1 - \exp(-\beta\Delta E)}\right]^{n_c^j(\Delta E, t)} \tag{9}$$

where the product is over all possible energy change ΔE due to the spin flip. In fact, the first term can be written as $\exp(-(\beta' - \beta)E_b^j(t))$. Here, $E_b^j(t)$ is to record the sum of the energy change in the case b of step 2 up to time t. For the nearest interaction, the number of ΔE is very small. Using this algorithm, we add nearly no extra computer time to a single simulation and in principle, can reweight the observables to any temperatures that need not to be predetermined.

2.3 Dynamic scaling analysis

In the last decade, it has been discovered that already in a macroscopic *short-time* regime emerges the universal scaling behavior. The physical origin of the scaling behavior is the divergent correlating time at the second-order phase transition. A dynamic scaling form which is valid up to the macroscopic short-time regime, has been derived with an ϵ-expansion up to two loop order by Janssen et al. [17,21], and its finite size form, e.g. for the k-th moment of the magnetization, is written as

$$M^{(k)}(t, \tau, L, m_0) = b^{-k\beta/\nu} M^{(k)}(b^{-z}t, b^{1/\nu}\tau, b^{-1}L, b^{x_0}m_0). \tag{10}$$

Here b is a rescaling factor, τ is the reduced temperature, β and ν are the static critical exponents and z is the dynamic exponent, while the new independent exponent x_0 is the scaling dimension of the initial magnetization m_0, and m_0 is assumed to be small around the fixed point $m_0 = 0$. It is important that from the scaling behavior of equation (10) it is possible to extract not only the dynamic exponent x_0 and z but also the static exponents and transition temperature originally defined in equilibrium. Since the non-equilibrium spatial correlation length at the early stage of the time evolution is small, the finite size effect can be easily controlled. Measurements now are carried out at the early stage of the time evolution, therefore one does not suffer from critical slowing down.

In general, for determination of the dynamic exponent z and static exponents, a dynamic process starting from a completely *ordered* state is more favorable, since fluctuation is less. In this case, the dynamic system is at another fixed point $m_0 = 1$ (in contrast to the fixed point $m_0 = 0$ relevant for Eq. (10)). The scaling variable m_0 now becomes irrelevant for the dynamic scaling behavior, and it can be simply removed from equation (10) [21]. Assuming the lattice is sufficiently large, the dynamic scaling form of the magnetization around the critical point is written as

$$M(t, \tau) = t^{-c_1} F(t^{1/\nu z}\tau), \qquad c_1 = \beta/\nu z\ . \tag{11}$$

If $\tau = 0$, the magnetization decays by a power law $M(t) \sim t^{-c1}$. If $\tau \neq 0$, the power-law behavior is modified by the scaling function $F(t^{1/\nu z}\tau)$. From this fact, one determines the critical point and the critical exponent $\beta/\nu z$. To estimate the exponent $1/(\nu z)$, we differentiate $\ln\ M(t, \tau)$ and obtain

$$\partial_\tau\ \ln\ M(t, \tau)|_{\tau=0} \sim t^{c_l}, \qquad c_l = 1/\nu z\ . \tag{12}$$

In order to measure the dynamic exponent z *independently*, we introduce a time-dependent Binder cumulant $U = M^{(2)}/M^2 - 1$, and the finite size scaling analysis shows

$$U(t, L) \sim t^{c_2}, \qquad c_2 = d/z \ . \tag{13}$$

For a magnetic system which is initially in a high-temperature state, suddenly quenched to the critical temperature T_c, and then released for the dynamic evolution, two interesting observables are the second moment of the magnetization and the auto-correlation function. For $\tau = 0$ and $m_0 = 0$, it is well known [18,21]

$$M^{(2)}(t) \sim t^y, \quad y = (d - 2\beta/\nu)/z. \tag{14}$$

Careful analysis [38] reveals that the auto-correlation function behaves like

$$A(t) \sim t^{-\lambda}, \qquad \lambda = d/z - (x_0 - \beta/\nu)/z. \tag{15}$$

Interesting here is that even though $m_0 = 0$, the exponent x_0 still enters the auto-correlation function. This behavior has been confirmed in a variety of statistical systems [18,21].

2.4 Dynamic criterion for weak first-order phase transitions

At the second-order transition temperature T_c, the short-time behavior of physical observables obeys a power law in dynamic processes starting from both a random and an ordered states. Away from T_c, the power-law behavior is modified by a scaling function [21]. If the phase transition is of first-order, independent of the initial states, physical observables at the transition temperature do not present a power-law behavior due to the finite correlating time and/or the symmetry breaking.

Around a first-order transition point, it is well known that for $K > K_c$ there is a disordered meta-stable state, which vanishes at a certain K^*. For $K < K_c$ there exists an ordered meta-stable state, which disappears at K^{**}. For a weak first-order phase transition, both K^* and K^{**} look like critical points if the system remains in the disordered and ordered meta-stable states, respectively. K^* and K^{**} are named disordered and ordered pseudo critical points respectively.

In equilibrium, numerical measurements of K^* and K^{**} are not easy due to finite-size effects. However, in the short-time dynamics, K^* and K^{**} can be determined relatively confidently. Starting from a high temperature state, the system at $K > K_c$ first reaches the disordered meta-stable state. Due to the large correlating time induced by the large spatial correlation length in the meta-stable state, physical observables at K^* present an approximate power-law behavior. The weaker the transition is, the cleaner the power-law behavior will be. This give an estimate of K^*. Starting from a zero temperature state, the system at $K < K_c$ first reaches the ordered meta-stable state and one can determine K^{**}. At a second-order phase transition, K^* and K^{**} overlap with the transition point K_c. Therefore, as Schülke and Zheng suggested [39], the difference of K^* an K^{**} gives a criterion for a weak first-order transition. This method has been successfully applied to a couple of physical systems [40,41].

3 Numerical simulations

We have performed Monte Carlo simulations with the standard Metropolis algorithm. The maximum updating time is taken to be from 500 to 3000 Monte Carlo time steps, depending on the lattice sizes and the specific observables. Large parts of results are presented with a lattice size $L = 40$. At the bond concentration $p = 0.56$, additional simulations have been performed for $L = 64$ and 96 to investigate possible finite size effects, and to extract more accurate exponents. Samples of the disordered couplings $\{K_{ij}\}$ for averaging are mostly from 5000 for the ordered start to 20 000 for the disordered start.

To estimate the errors, total samples are divided into three or four subgroups. Statistical errors are then calculated from independent measurements of these subgroups of samples. In addition, results of the measurements may fluctuate also for different time windows $[t_1, t_2]$ in which the measurements are performed. These errors will be taken into account, if they are comparable to statistical errors. Corrections to scaling are carefully considered.

3.1 The tricriticality

In references [15,16], the disorder-induced tricritical point was estimated between bond dilutions $p = 0.68$ and $p = 0.84$, and below the tricritical point the transition is softened to second order. We start our simulations with $p = 0.78$. In Figure 1a, the magnetization with an ordered initial state is obtained from simulations at a single temperature $K = 0.80415$ and then reweighted to the temperatures $K = 0.8043$ and 0.8040; the average is taken over 5000 samples. Searching for a temperature, with which the curve exhibits the best power-law-like behavior, one determines the ordered pseudo critical point $K^{**} = 0.80414(6)$. In order to confirm the dynamic reweighting approach, we have also performed simulations at $K = 0.8043$ and 0.8040 and compared the data with the reweighting ones from the simulation at $K = 0.80415$. This is shown in Figure 1a. Within fluctuations, the curves from direct simulations overlap with those from reweighting. In Figure 1b, simulations are performed at $K = 0.8050$, 0.8046 and 0.8042 with disordered starts, and $K^* = 0.80468(13)$ is estimated from $M^{(2)}(t)$. Obviously, K^* is bigger than K^{**}, and this indicates that the phase transition is of first order. For a second-order phase transition, K^* and K^{**} overlap.

Carefully decreasing the bond concentration, at $p = 0.76$ we obtain $K^{**} = 0.82541(6)$ and $K^* = 0.82558(7)$ from $M(t)$ and $M^{(2)}(t)$, as shown in Figure 2 respectively. Taking into account the errors, one may still observe $K^{**} < K^*$, and the phase transition remains as a first-order one although the discontinuity is very weak [39].

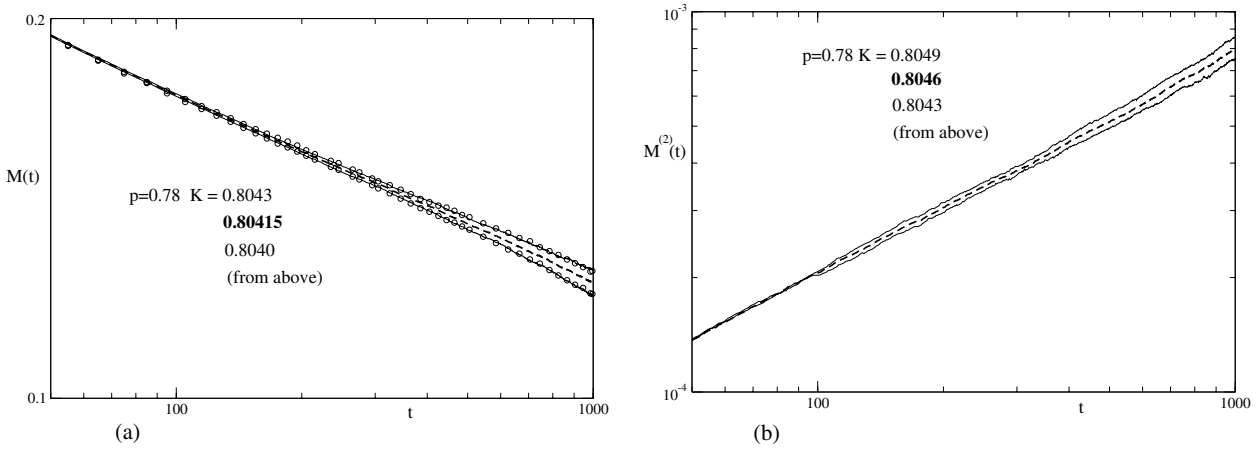

Fig. 1. The magnetization and second moment for the bond concentration $p = 0.78$ with a lattice size $L = 40$ plotted vs. t on a log-log scale: (a) $M(t)$ with an ordered start, obtained with the dynamic reweighting method from simulations at a single temperature $K = 0.80415$. The dash line is the closest to the pseudo critical point K^{**}. For comparison, other two direct simulations at temperatures $K = 0.8043$ and 0.8040 are displayed with circled lines. (b) $M^{(2)}(t)$ with a disordered start from simulations at three different temperatures $K = 0.8050$, 0.8046 and 0.8042. The dash line is the closest to the pseudo critical point K^*.

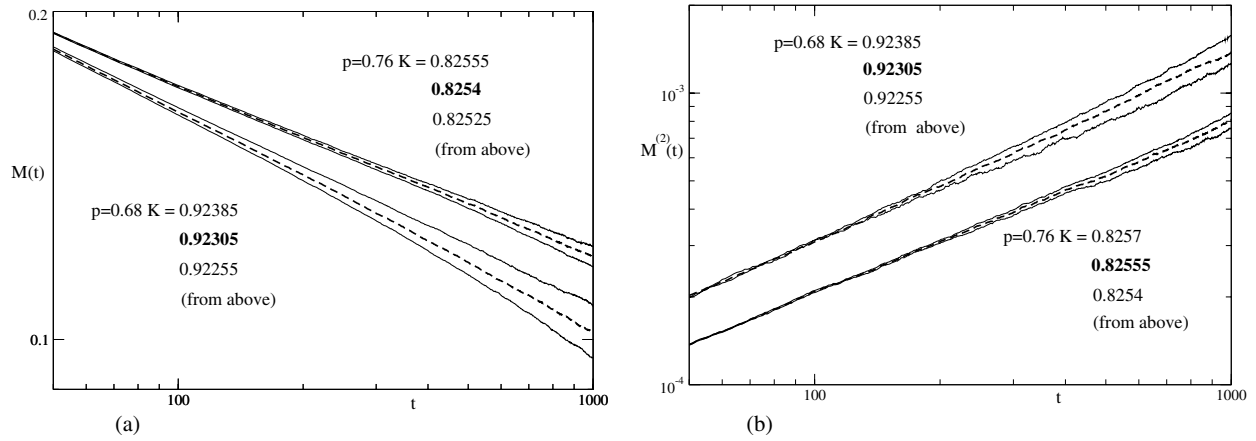

Fig. 2. The magnetization and second moment for $p = 0.68$ and $p = 0.76$ with a lattice size $L = 40$ plotted vs. t on a log-log scale: (a) $M(t)$ with an ordered start from simulations at a single temperature $K = 0.82535$ for $p = 0.76$, and at three different temperatures $K = 0.9238$, 0.9230 and 0.9224 for $p = 0.68$, respectively. The dash line is the closest to the pseudo critical points K^{**}. (b) $M^{(2)}(t)$ with a disordered start from simulations at a single temperature $K = 0.8256$ for $p = 0.76$, and at three different temperatures $K = 0.9238$, 0.9230 and 0.9224 for $p = 0.68$. The dash line is the closest to the pseudo critical point K^*.

The same process is applied to $p = 0.68$. The magnetization and second moment with an ordered and a disordered start are plotted in Figure 2, respectively. Carefully analyzing the data from simulations, we find out $K^* = 0.92310(23)$ and $K^{**} = 0.92315(32)$. The values of the pseudo critical points K^* and K^{**} overlap within the error bars, and this shows that the phase transition is rounding to a continuous one. Clearly, there exists a tricritical point between $p = 0.68$ and 0.76, i.e. $p_c = 0.72(4)$.

To obtain a more accurate estimate of the tricritical point, we also perform simulations at $p = 0.72$. The crossover effect is a little stronger when p is close to the tricritical point, but we can extract $K^* = 0.87145(17)$ and $K^{**} = 0.87141(19)$, which indicates that the transition is of second order. So, more accurately, the tricritical point is expected at $p_c = 0.74(2)$. All the results of K^*, and K^{**} are summarized in Table 1. The critical temperature K_c of second order transitions can be calculated from $(K^*+K^{**})/2$, and $(K^*+K^{**})/2$ also give a good estimate of transition points for weak first-order transitions [39].

Here we should mention that since the bond concentrations we investigate are rather close to the tricritical point, corrections to scaling are relatively strong especially for the simulations with the ordered initial state [42]. Therefore, in order to extract the pseudo critical points reliably, we sometimes perform simulations at a couple of temperatures and then interpolate the data to other temperatures to estimate $K^{**}s$ and K^*s. In order to measure the

Table 1. Pseudo critical points K^{**} and K^{*} measured with the short-time dynamic approach for the 3D bond-diluted 4-state Potts model at different bond concentrations p. The tricritical point is estimated to be $p_c = 0.74(2)$.

	$p = 0.44$	$p = 0.56$	$p = 0.68$	$p = 0.72$	$p = 0.76$	$p = 0.78$
K^{**}	1.4821(3)	1.1298(4)	0.92315(32)	0.87141(19)	0.82541(6)	0.80414(8)
K^{*}	1.4822(2)	1.1301(5)	0.92310(23)	0.87145(17)	0.82558(7)	0.80468(13)

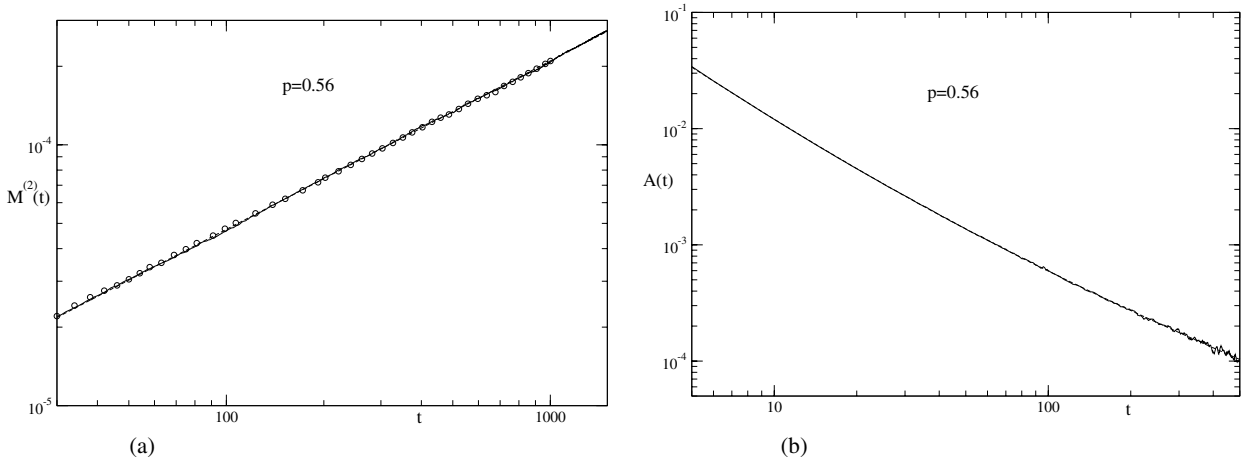

Fig. 3. The second moment and auto-correlation function with a disorder start for $p = 0.56$ plotted vs. t on a log-log scale: (a) $M^{(2)}(t)$ is plotted with a solid line for a lattice size $L = 64$. The dashed line shows a power-law fit. The circled line is for a lattice size $L = 40$ to a maximum time $t = 1000$. (b) $A(t)$ is plotted with a solid line for a lattice size $L = 64$. The dashed line shows a fit with corrections to scaling.

critical exponents for the continuous transition at $p = 0.68$ as it will be discussed in the next subsection, we reweight the data at the temperature from direct simulations to the critical points, and then considered the corrections to scaling.

3.2 Critical exponents of the continuous phase transition

Now let us concentrate on the critical properties of disorder-induced continuous transitions. We start our simulations at the bond concentration $p = 0.56$. Since $p = 0.56$ is away from both the percolation transition point and tricritical point, corrections to scaling are relatively small. In Figure 3, the second moment and autocorrelation directly measured at critical points with a disordered start are displayed with solid lines on a log-log scale. The simulations are performed up to a maximum updating time 1500 with a lattice size $L = 64$, and the averages are taken over 24 000 samples. In Figure 3a, $M^{(2)}(t)$ exhibits a perfect power-law behavior in equation (14) in a time interval $[t_1, t_2] = [30, 1500]$. Thus the exponent $y = (d - 2\beta/\nu)/z = 0.646(3)$ can be estimated from the slope of the curve. Corrections to scaling are not needed here.

In order to examine the possible finite size effect and confirm our results, simulations at the same temperature have been performed with a lattice size $L = 40$ up to a maximum time 1000, as shown with circled line in Figure 3a. Obviously, within 1000 time steps, the curves of $L = 40$ and 64 overlap each other within fluctuations. According to the finite-size scaling theory, the time scale for the finite size effect is $\sim L^z$. At $p = 0.56$, the dynamic exponent z is estimated to be 2.60(5) as discussed below. Therefore, negligible finite-size effects are expected for the data of $L = 64$ in the time regime in Figure 3a.

The autocorrelation function is plotted in Figure 3b. Corrections to scaling are rather strong even looking by eyes. Therefore, we fit the curve to the form of $A(t) \sim t^{-\lambda}(1+c/t^b)$ according to equation (15). A good fit of $A(t)$ is found in the time interval $[5, 500]$, and the exponent $\lambda = d/z - (x_0 - \beta/\nu)/z$ and correction exponent b are estimated to be $\lambda = 0.948(15)$ and $b = 0.43$, respectively. The fluctuation beyond $t = 500$ is very large since the exponent λ is big.

Further, we turn to simulations with an ordered initial state at $p = 0.56$. The fluctuation of the dynamic variables in this process is less than that with a disordered start. However, corrections to scaling are relatively stronger. In Figure 4a, the magnetization and Binder Cumulant are displayed on a double-log scale. Simulations are performed with a lattice size up to 96 and a maximum time up to 3000; averages are taken over 7000 samples. Due to the cross-over effect, corrections to scaling of $M(t)$ and $U(t)$ are detected in the early times. Thus, in Figure 4a we fit the curve of $M(t)$ to the form of $M(t) \sim t^{-\beta/\nu z}(1 + c/t^b)$ according to equation (11). The correction exponent b for $M(t)$ is about 0.05. The small correction exponent b indicates that one may also fit the curve with a logarithmic correction to scaling, $M(t) \sim t^{-\beta/\nu z}(1 + cln\ t)$. Actually,

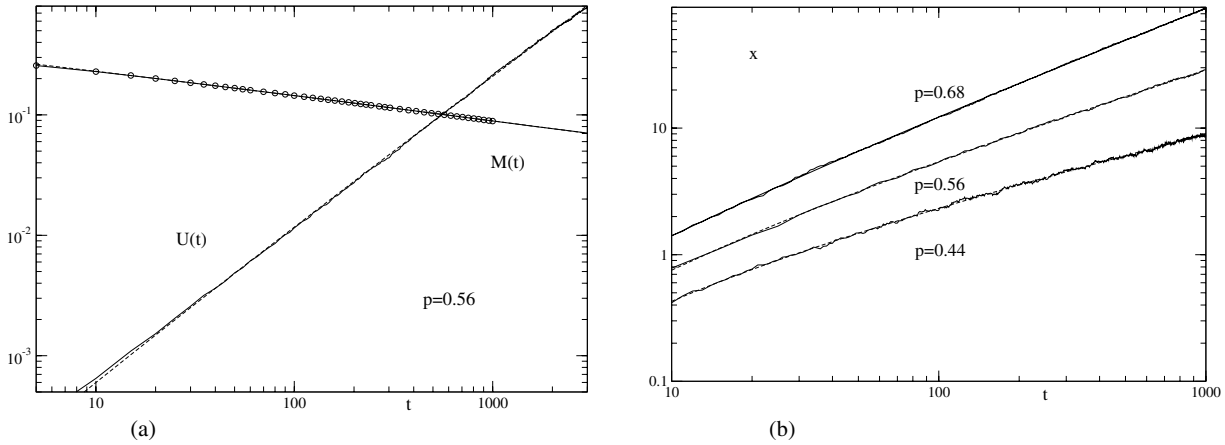

Fig. 4. The magnetization, Binder cumulant and $\partial_\tau \ln M(t,\tau)|_{\tau=0}$ with an order start plotted vs. t on a log-log scale: (a) $M(t)$ and $U(t)$ are plotted with solid lines for $p = 0.56$ with a lattice size $L = 96$. Dashed lines show fits with corrections to scaling. The circled line is for a lattice size $L = 40$ to a maximum time $t = 1000$. (b) $\partial_\tau \ln M(t,\tau)|_{\tau=0}$ is plotted with solid lines for $p = 0.44$, 0.56 and 0.68 with a lattice size $L = 40$. Dash lines show fits with corrections to scaling.

fitting with a logarithmic correction is more stable than a power-law correction. From the exponent $\beta/\nu z = 0.250(2)$ estimated here and $y = (d - 2\beta/\nu)/z = 0.646(3)$ obtained in the dynamic process with a disordered start, we can determine the static exponent $\beta/\nu = 0.654(14)$ and the dynamic exponent $z = 2.62(3)$.

Similar as the cases with a disordered start, simulations are also performed for $M(t)$ with an ordered start and with a lattice size $L = 40$ and the maximum time $t = 1000$, as displayed with the circled line in Figure 4a. The curves for both $L = 40$ and 96 coincide well within 1000 time steps, and it shows that the finite size effect is negligible small in the time regime $[10, 3000]$ for a lattice size $L = 96$.

In Figure 4a, the time-dependent Binder cumulant is fitted to the form of $U(t) \sim t^{d/z}(1 + c/t^b)$ according to equation (13), in order to extract the dynamic exponent z independently. The result $z = 2.60(4)$ is in good agreement with $z = 2.62(3)$ obtained from $c_1 = \beta/\nu z$ and $y = (d - 2\beta/\nu)/z$ above. Here the exponent $b = 0.13$ is also rather small.

To estimate the index $c_l = 1/\nu z$ from equation (12), we perform simulations at temperatures in the neighborhood of the transition point to approximate the differentiation of $\ln M(t,\tau)$. As usual, relatively large corrections to scaling are detected. In Figure 4b, the curve is fitted to the form of $\partial_\tau \ln M(t,\tau)|_{\tau=0} \sim t^{1/\nu z}(1 + c/t^b)$. The exponent b is estimated to be 0.18. All our measurements of the indices y, λ, $c1$, c_l and $c2$ at $p = 0.56$ are summarized in Table 2. To deduce the static exponents β/ν and $1/\nu$, an averaged value $z = 2.61$ of the dynamic exponent is used.

Finally, we have performed simulations at $p = 0.44$ and 0.68 to complete our study in the second order regime. The data at critical points are reweighted from simulations at $K = 1.14218$ and 0.92305 for $p = 0.44$ and 0.68, respectively. The same power-law corrections to scaling are applied to extract the critical exponents. In Figure 5, the curves of $M^{(2)}(t)$ and $A(t)$ with disordered starts are shown in solid lines with a double-log scale. At $p = 0.44$, just like the case of $p = 0.56$, corrections of $M^{(2)}(t)$ are negligible and a nice power-law is observed in the time interval $[20, 1000]$, as shown in Figure 5a. But corrections to scaling seem to be stronger for $p = 0.68$. To extract the exponent, the corrections to scaling have to be taken into account. We estimated the correction exponent $b = 0.44$ for $A(t)$ at $p = 0.44$, and 0.15 for $M^{(2)}(t)$ at $p = 0.68$.

In Figure 5b, due to rather strong cross-over effects and large fluctuations even after $t = 100$ for $p = 0.68$, we could not fit the curve of $A(t)$ stably in such a limited time regime. As to the $M(t)$ and $U(t)$ with an ordered initial state, good fits can be clearly seen in Figure 6. The curves of $\partial_\tau \ln M(t,\tau)|_{\tau=0}$ are plotted in Figure 4b. Here the exponent b for $M(t)$, $U(t)$ and $\partial_\tau \ln M(t,\tau)|_{\tau=0}$ are 0.07, 0.21 and 0.16 for $p = 0.44$, and 0.12, 0.35 and 0.19 for $p = 0.68$. All the results of $p = 0.44$ and 0.68 are also summarized in Table 2.

Table 2. Critical exponents of the 3D bond-diluted 4-state Potts model at different bond concentrations p, measured from the dynamic observables $M^{(2)}(t)$, $A(t)$, $M(t)$, $U(t)$ and $\partial_\tau \ln M(t,\tau)|_{\tau=0}$, respectively, starting from both the ordered and disordered initial states.

	m_0	$p = 0.44$	$p = 0.56$	$p = 0.68$
$y = (d - 2\beta/\nu)/z$	0.0	0.587(4)	0.646(3)	0.950(17)
λ		0.895(7)	0.948(15)	
$c_1 = \beta/\nu z$	1.0	0.173(3)	0.250(2)	0.257(5)
$c_2 = d/z$		0.923(21)	1.153(17)	1.493(42)
$c_l = 1/\nu z$		0.433(15)	0.546(11)	0.711(8)
$z = d/c_2$		3.25(8)	2.60(4)	2.01(6)
$z = d/(y + 2c_1)$		3.22(4)	2.62(3)	2.05(4)
$\beta/\nu = zc_1$		0.56(2)	0.653(14)	0.522(23)
$1/\nu = zc_l$		1.40(9)	1.425(51)	1.443(57)

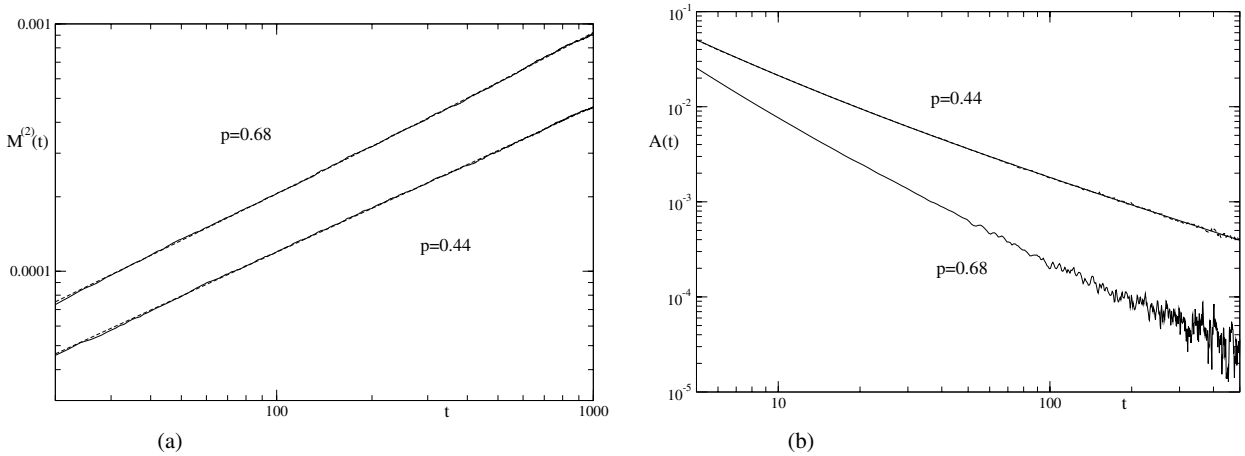

Fig. 5. The second moment and auto-correlation function with a disorder start for a lattice size $L = 40$ plotted vs. t on a log-log scale: (a) $M(t)$ is plotted with solid lines for $p = 0.44$ and $p = 0.68$. Dashed lines show a power-law fit for $p = 0.44$ and a fit with corrections to scaling for $p = 0.68$. (b) $A(t)$ is plotted with solid lines for $p = 0.44$ and $p = 0.68$. The dashed line shows a fit with corrections to scaling for $p = 0.44$.

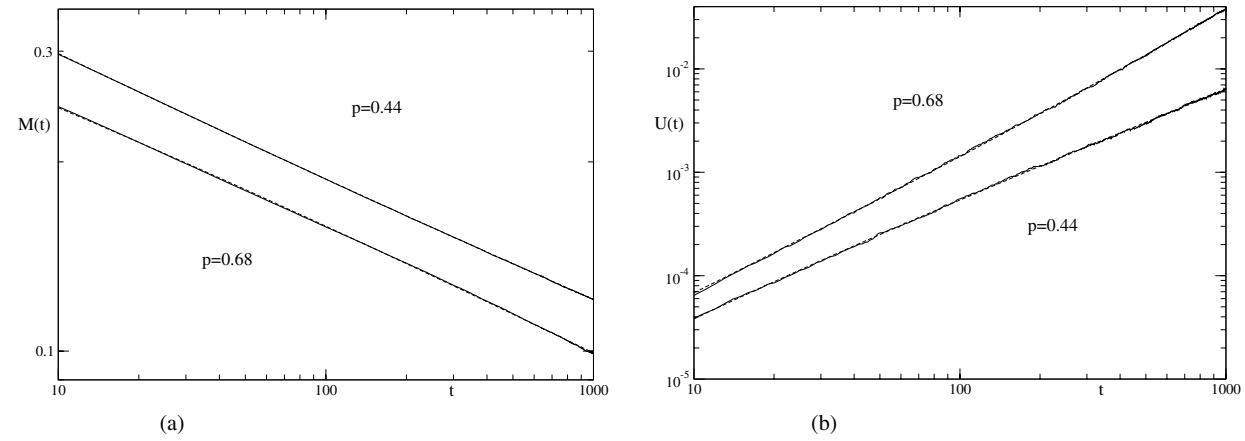

Fig. 6. The magnetization and Binder cumulant with an order start for a lattice size $L = 40$ and $p = 0.44$ and 0.68 plotted vs. t on a log-log scale: (a) $M(t)$ is plotted with solid lines. Dashed lines show fits with corrections to scaling. (b) $U(t)$ is plotted with solid lines. Dashed lines show fits with corrections to scaling.

In summary, our results support the existence of a tricritical point between the bond concentrations $p = 0.68$ and 0.84 reported in references [15,16], and with the short-time dynamic approach, we obtain a relatively more accurate tricritical point $p_c = 0.74(2)$. For $p = 0.56$, the static exponent $\beta/\nu = 0.653(14)$ is in good agreement with $\beta/\nu = 0.65(5)$ extracted from the finite size scaling in equilibrium with lattices up to $L = 96$ in reference [15]. For $p = 0.44$ and 0.68, the exponent β/ν takes values 0.56(2) and 0.522(23) respectively, which should be compared with 0.534(14) and 0.547(51) obtained from simulations in equilibrium with lattices up to $L = 128$ for $p = 0.44$ and $L = 64$ for $p = 0.68$ [16]. The non-monotonous behavior of β/ν may be considered as the effect of the percolation point $p = 0.2488126(5)$ [43] and tricritical point $p = 0.74(2)$, and expects a random fix point in between [16].

Our estimate of the critical exponent ν shows rather weak dependence on the bond concentration p, and $1/\nu$ takes values 1.40(9), 1.425(51) and 1.443(57) for $p = 0.44$, $p = 0.56$ and $p = 0.68$ respectively. These values are somewhat bigger than 1.36(2), 1.33(3) and 1.38(8) reported in reference [16], but closer to $1/\nu = 1.462(11)$ for the 3D site-diluted Ising model [44], and $1/\nu = 1.449(11)$ for the 3D site-diluted 3-state Potts model [14]. In addition, we also provide the dynamic exponents z and λ, and the dynamic exponent z is bond concentration p dependent. Different from the case of β/ν, the dependence of z on p is monotonous. This should be understandable for the dynamics should become slower as p decreases.

In reference [16], an extrapolation from finite lattices to $L \to \infty$ is suggested, and for $p = 0.56$, the extrapolated exponents are $\beta/\nu = 0.732(24)$ and $1/\nu = 1.339(25)$. Since we have considered the corrections to the scaling in

the time direction, here we do not try to perform a similar extrapolation to the limit $t \to \infty$. Actually, how to carry out the extrapolation is not very unique and might contain also certain uncertainty. In the short-time dynamic approach, the finite size effect is negligibly small for the lattices and time regimes we investigate.

4 Conclusion

With extensive Monte Carlo simulations, we investigate the short-time dynamics of the three-dimensional bond-diluted 4-state Potts model. Special attention is given to the effect of disorder on the rounding of the phase transitions of, and a relatively accurate estimate of the tricritical point $p_c = 0.74(2)$ is obtained. In the second-order phase transition regime, we study the critical behavior at three bond concentrations p, and corrections to scaling are carefully taken into account. We make an attempt to improve the recently suggested nonequilibrium reweighting method, and apply it to the short-time dynamic Monte Carlo simulations. The dynamic approach shows its merit in estimating the pseudo critical points K^* and K^{**} around a weak first-order phase transition, and in tackling the dynamic and static properties of disordered systems.

This work was supported in part by NNSF and SRFDP (China), DFG (Germany) and RFBR (Russia) through grants No. 04-02-17524 and No. 04-02-39000.

References

1. Y. Imry, M. Wortis, Phys. Rev. B **19**, 3580 (1979)
2. K. Hui, A.N. Berker, Phys. Rev. Lett. **62**, 2507 (1989)
3. M. Aizenman, J. Wehr, Phys. Rev. Lett. **62**, 2503 (1989)
4. S. Chen, A.M. Ferrenberg, D.P. Landau, Phys. Rev. E **52**, 1377 (1995)
5. M. Picco, Phys. Rev. B **54**, 14930 (1996)
6. J. Cardy, J.L. Jacobsen, Phys. Rev. Lett. **79**, 4063 (1997)
7. C. Chatelain, B. Berche, Phys. Rev. Lett. **80**, 1670 (1998)
8. T. Olson, A.P. Young, Phys. Rev. B **60**, 3428 (1999)
9. C. Chatelain, B. Berche, Nucl. Phys. B **572[FS]**, 626 (2000)
10. C. Deroulers, A.P. Young, Phys. Rev. B **66**, 014438 (2002)
11. J.Ch. Anglés d'Auriac, F. Iglói, Phys. Rev. Lett. **90**, 190601 (2003)
12. J.Q. Yin, B. Zheng, S. Trimper, Phys. Rev. E **70**, 056134 (2004)
13. K. Uzelac, A. Hasmy, R. Jullien, Phys. Rev. Lett. **74**, 422 (1995)
14. H.G. Ballesteros, L.A. Fernández, V. Martín-Mayor, A. Muñoz Sudupe, G. Parisi, J.J. Ruiz-Lorenzo, Phys. Rev. B **61**, 3215 (2000)
15. C. Chatelain, B. Berche, W. Janke, P.E. Berche, Phys. Rev. E **64**, 036120 (2001)
16. C. Chatelain, B. Berche, W. Janke, P.E. Berche, Nucl. Phys. B **719**, 275 (2005)
17. H.K. Janssen, B. Schaub, B. Schmittmann, Z. Phys. B **73**, 539 (1989)
18. D.A. Huse, Phys. Rev. B **40**, 304 (1989)
19. K. Humayun, A.J. Bray, J. Phys. A **24**, 1915 (1991)
20. Z.B. Li, U. Ritschel, B. Zheng, J. Phys. A **27**, L837 (1994)
21. B. Zheng, Int. J. Mod. Phys. B **12**, 1419 (1998), review article
22. B. Zheng, M. Schulz, S. Trimper, Phys. Rev. Lett. **82**, 1891 (1999)
23. D. Stauffer, Physica A **186**, 197 (1992)
24. N. Ito, Physica **A 196**, 591 (1993)
25. H.J. Luo, L. Schülke, B. Zheng, Phys. Rev. Lett. **81**, 180 (1998)
26. N. Ito, Y. Ozeki, Physica A **321**, 262 (2003)
27. B. Zheng, in *Computer Simulation Studies in Condensed-Matter Physics XVII*, edited by D.P. Landau (Springer, Heidelberg, 2004)
28. H.J. Luo, L. Schülke, B. Zheng, Mod. Phys. Lett. B **13**, 417 (1999)
29. H.J. Luo, L. Schülke, B. Zheng, Phys. Rev. E **64**, 36123 (2001)
30. Y. Ozeki, N. Ito, Phys. Rev. B **64**, 024416 (2001)
31. A.M. Ferrenberg, R.H. Swendsen, Phys. Rev. Lett. **61**, 2635 (1988)
32. J.S. Wang, R.H. Swendsen, R. Kotechý, Phys. Rev. Lett. **63**, 109 (1989)
33. T.P.P.M.C. de Oliveira, H. Herrmann, Braz. J. Phys. **26**, 677 (1996)
34. F. Wang, D.P. Landau, Phys. Rev. Lett. **86**, 2050 (2001)
35. J.S. Wang, R.H. Swendsen, J. Stat. Phys. **106**, 245 (2002)
36. R. Dickman, Phys. Rev. E **60**, R2441 (1999)
37. H.K. Lee, Y. Okabe, Phys. Rev. E **71**, 015102(R) (2005)
38. H.K. Janssen, in *From Phase Transition to Chaos*, edited by G. Györgyi, I. Kondor, L. Sasvári, T. Tél, *Topics in Modern Statistical Physics* (World Scientific, Singapore, 1992)
39. L. Schülke, B. Zheng, Phys. Rev. E **62**, 7482 (2000)
40. E.V. Albano, Phys. Lett. A **288**, 73 (2001)
41. G.P. Saracco, E.V. Albano, J. Chem. Phys. **118**, 4157 (2003)
42. G.P. Zheng, M. Li, Phys. Rev. E **65**, 036130 (2002)
43. C.D. Lorenz, R.M. Ziff, Phys. Rev. E **57**, 230 (1998)
44. H.G. Ballesteros, L.A. Fernández, V. Martín-Mayor, A. Muñoz Sudupe, G. Parisi, J.J. Ruiz-Lorenzo, Phys. Rev. B **58**, 2740 (1998)